Available online at www.sciencedirect.com
SCIENCE DIRECT®
ELSEVIER
Applied Surface Science 208–209 (2003) 2–14
applied surface science
www.elsevier.com/locate/apsusc

Synergistic effects of exposure of surfaces of ionic crystals to radiation and water

J.T. Dickinson[a,*], Khin Hla Nwe[a], W.P. Hess[b], S.C. Langford[a]

[a]*Surface Dynamics Laboratory, Physics Department, Washington State University, Pullman, WA 99164-2814, USA*
[b]*Pacific Northwest National Laboratory, Richland, WA 99352, USA*

Abstract

We present studies of the consequences of simultaneous exposure of inorganic single crystals to radiation and water. The first case consists of a biomineral, $CaHPO_4{\cdot}2H_2O$ (brushite), which is a wide band gap, hydrated inorganic single crystal. We examine the laser-induced ion and neutral emissions accompanying 248 nm excimer laser radiation. Both types of emission are several orders of magnitude higher following exposure to 2 keV electrons at current densities of 200 $\mu A/cm^2$ and doses of 10^2 to 10^3 mC/cm^2. We show that the enhancements in emission are strongly correlated with e-beam induced morphology changes (including recrystallization) on this unusual surface. We then examine similar effects on ''dry'' crystals such as NaCl and $NaNO_3$ which are exposed to 10^{-5} Pa partial pressures of H_2O. Again dramatic enhancements in radiation induced emissions are exhibited along with the generation of unique morphological structures with nanometer scale dimensions.

Keywords: Laser desorption; Defects; Hydrated single crystal; Biomineral; Surface modification; Electron stimulated desorption; Water vapor; Nanostructures; Nanotechnology

1. Introduction

When two stimuli are applied to a system simultaneously one always has the possibility of a synergism, i.e. where the total result is greater than the sum of the individual effects. We have shown in the past that such synergisms arise when we combine exposure of materials to mechanical stress and electron beam irradiation (e-beam irradiation) [1,2], chemical exposure and e-beam irradiation [3–7], electron and laser beams [8–10], and mechanical and chemical stimulation [11–14], all of which are cloaked in what we sometimes call our ''one-two punch''. Here we would like to examine the possible role water can play in changing rates of radiation induced desorption and decomposition on single crystals. For soluble inorganic materials, water can be considered somewhat aggressive in that when sorbed on such a surface, the oriented dipoles of the water can exert forces on lattice ions/atoms and lower their binding energies. This is particularly effective at defect sites such as steps and kinks because these structures correspond to lower coordination (therefore lower binding energy) and water can better surround (solvate) the ions at these sites. This results again in stronger forces and lowered binding energies. In addition, many defects on ionic crystals are chemically active and promote dissociation of the water leading to sorbed H and OH. Examples are MgO [15] and TiO_2 [16] where anion vacancies are shown to dominate the reactions.

* Corresponding author. Tel.: +1-509-335-4914; fax: +1-509-335-7816.
E-mail address: jtd@wsu.edu (J.T. Dickinson).

0169-4332/02/$ – see front matter
PII: S0169-4332(02)01277-1

Very little work has been done on the influence of electron and laser irradiation on inorganic crystalline materials that contain waters of hydration. Such structures are common in the environment as well as in a number of biologically derived materials. The surfaces of such crystals can be dramatically altered by UV and electron irradiation. Single crystal $CaHPO_4{\cdot}2H_2O$ (brushite) is a wide band gap, UV transparent, inorganic phosphate biomineral with applications in dentistry, medical implants, and prosthetic devices, as well as serving as a possible target material for laser surface modification and pulsed laser deposition of biocompatible materials. Here we compare mass-selected measurements of laser-desorbed ions and neutral molecules from as-grown or as-cleaved surface with measurements from electron-irradiated surfaces (2 keV electrons at current densities of $\sim$200 μA/cm^2 and doses of $\sim 10^2$ to 10^3 mC/cm^2). As-cleaved brushite crystals are transparent and quite resistant damage by 30 ns pulses of 5 eV photons (KrF excimer laser, 248 nm). However, prior exposure to the electron beam creates defects that dramatically increase the surface–laser interaction and the resulting ionic and neutral products.

Likewise, little work has been done on the influence of background water present during irradiation of ionic crystals with electron and laser beams. We present our results of such irradiation in background pressures of water $\sim 10^{-5}$ Pa. Strong synergisms are revealed and we suspect that water vapor is enhancing defect moderated emission processes.

2. Experiment

Single crystals of monoclinic brushite were grown from aqueous solutions of $Ca(NO_3)_2$ and $NH_4(H_2PO_4)$ by slow diffusion in dilute nitric acid (pH 2–4) at room temperature [17]. The resulting plate-like crystals were stored in saturated solution and exposed to air only when mounted in the vacuum chamber. As-grown crystals and crystals cleaved minutes before placing in the vacuum system showed very similar emissions. All work on brushite was carried out at a nominal crystal temperature of 25 °C. Melt grown single crystals of $NaNO_3$ were grown in our laboratory by heating 99.0% pure $NaNO_3$ powder (mp: 306.8 °C) in air to 315 °C and then slowly, over a period of several days, cooling it back down to room temperature. Transmission measurements obtained using a Lambda 900, Perkin-Elmer UV-Vis/NIR spectrometer, and a 400 μm thick melt grown $NaNO_3$ single crystal, as well as X-ray and ultraviolet photoelectron emission experiments [18] resulted in spectra similar to those reported in the literature [19–23]. Optical grade, high purity NaCl crystals were purchased from Optovac Inc. Both the $NaNO_3$ and NaCl crystals were cleaved in air before mounting in the vacuum system. The cleavage process is known to generate significant densities of surface defects including vacancies, steps, and kinks. The sample holder was capable of heating the crystals to temperatures as high as 900 K.

The electron source was a Varian Model 981-2455 Auger electron gun operated at an electron kinetic energy of 2 keV and a current density of 100–200 μA/cm^2. A Lambda Physik LEXtra 200 provided 30 ns pulses of excimer laser radiation at 248 nm (KrF). The laser intensity was controlled with a MICROLAS Laser systems variable attenuator. The laser beam was focused by a quartz lens (focal length 35 cm) onto the sample at an angle of 20° with respect to the surface normal. Experiments were performed in a system with a background pressure of 10^{-10} Torr. The emitted particles during both electron and laser beam irradiation were detected with a UTI 100C quadrupole mass spectrometer (QMS) mounted with its axis along the surface normal. The QMS mass filter was tuned to a specific mass/charge ratio and the output detected as a function of time. Neutral particles were ionized by electron impact in the QMS ionizer operated at 70 eV and 2 mA emission. The resulting ions were drawn into the mass filter section, mass selected, and detected with a Channeltron Electron Multiplier (CEM). Measurements of mass-selected ion emission were made by grounding the electron optics at the entrance of the QMS (ionizer filaments, grids, and the focus plate). The CEM output was amplified by an Ortec Model 474 timing filter amplifier (<10 ns rise time), and then discriminated and counted by an EG&G Model 914P Multiple-Channel Scaler.

For the laser desorption of ions, time-of-flight (TOF) curves were fit to Gaussian energy distributions with one or occasionally two peaks, which, when transformed into TOF-space, take the form

$$I(t) = \frac{Amd^2}{t^3} \exp\left[\frac{-(E - md^2/2t^2)}{2\sigma^2}\right] \quad (1)$$

where d is the distance between the sample surface and the CEM (28 cm), m the ion mass, t the ion time-of-flight; E the mean kinetic energy, σ the standard deviation of the kinetic energy distribution; and A a constant.

For neutral particles emitted in thermal equilibrium from a surface at a temperature T, the time required to reach the QMS ionizer is described by a ''half-range'' Maxwell–Boltzmann distribution. After accounting for the time required for ions generated in the QMS ionizer to pass through the mass filter, this distribution takes the form

$$I(t) = \frac{\alpha m^2 d^2}{2\pi (kT)^2 t^4} \int_{\Delta V} \boldsymbol{r}_x \exp\left[\frac{-m\boldsymbol{r}^2}{2kTt^2}\right] \mathrm{d}V \qquad (2)$$

where α is the ionizer efficiency, m the particle mass, and k the Boltzmann constant. The integral is performed over the volume of the ionizer, ΔV, where $\boldsymbol{r}$ the position vector (with origin at the sample) and $\boldsymbol{r}_x$ the component of the position vector normal to the sample surface. Fits were performed only on the first 500 μs of data to avoid signals due to particles which have bounced off vacuum system walls. With a beam block between the sample and QMS ionizer, detectable signals due to particles reaching the detector via indirect paths were not observed during the first 500 μs after the laser pulse. To minimize the contribution of ion emissions to the neutral signals at high fluences, a negatively biased needle between two positively biased (or grounded) grids was positioned in front of the QMS ionizer for some measurements.

3. Results and discussion

3.1. Brushite: laser-induced ion emissions

Ca^+ is the principal cation observed from as-cleaved samples, followed by CaO^+ and PO^+. Electron-irradiated surfaces yielded these same ions, but several orders of magnitude more intense; in addition, electron-irradiated surfaces also yielded P^+. Fig. 1 compares the fluence dependence of the Ca^+, CaO^+, PO^+ emission intensities from as-cleaved samples with those from the same samples after exposure to electron doses of approximately 0.43 C/cm^2. All signals show highly non-linear behaviors, with slopes (on log–log plots) ranging from 4 to 10. Somewhat lower slopes are observed after electron irradiation. As reported previously for a number of ionic crystals [24] and for brushite [10], the laser desorption of positive ions is best described as a multiple photon process (a sequence of excitations) [24–26]. In this scenario, a sorbed adion is launched when a nearby electron trap is emptied, leading to the Coulomb repulsion necessary to push the ion away. For adion-trap separations on the order of one lattice spacing, we estimate that 1–2 charges must be removed from the trap to account for the observed ion energies. Defect complexes are required to account for the emission of molecular ions. P^+ emission (Fig. 1(d)) is detected only from electron-irradiated surfaces.

The Ca^+ intensities from all samples are characteristically orders of magnitude higher than those of CaO^+, PO^+, and P^+. Typical mean kinetic energies for electron-irradiated brushite are: Ca^+: 6 eV; CaO^+: 1 eV; PO^+ 3–4 eV and P^+: 5–6 eV. Thus the average ion kinetic energy often exceeds the 5 eV photon energy. Molecular ion emissions [27] from a number of ionic crystals (e.g., MgO, NaCl, and $NaNO_3$) show non-linear fluence dependencies; further, the polyatomic ions display distinctly lower kinetic energies than the atomic cations. These measurements were made at fluences low enough to ensure that the observed ions are emitted directly from the surface and are not produced by ionization of neutral particles.

3.2. Effect of electron irradiation on the surface

Brushite has a layered structure consisting of alternating layers of $CaHPO_4$ and H_2O [28]. These layers are parallel to the cleavage plane, allowing near-surface water to diffuse to the surface under vacuum conditions. Electron-induced heating generates subsurface voids due to the expansion of water vapor. These cavities serve as incubation sites for efflorescence [29–34] and recrystallization, resulting in the growth of tiny platelets and feathery structures. The rapid formation of these recrystallized structures is expected to yield high defect densities.

Previous FT-IR and XPS observations [10,35] indicate that electron-irradiated surfaces are principally composed of pyrophosphate ($P_2O_7^{4-}$); exposed voids are typically composed of recrystallized phosphate, PO_4^{3-} in contrast to both HPO_4^{3-} and $P_2O_7^{4-}$. Large delaminated areas are observed in SEM images of an

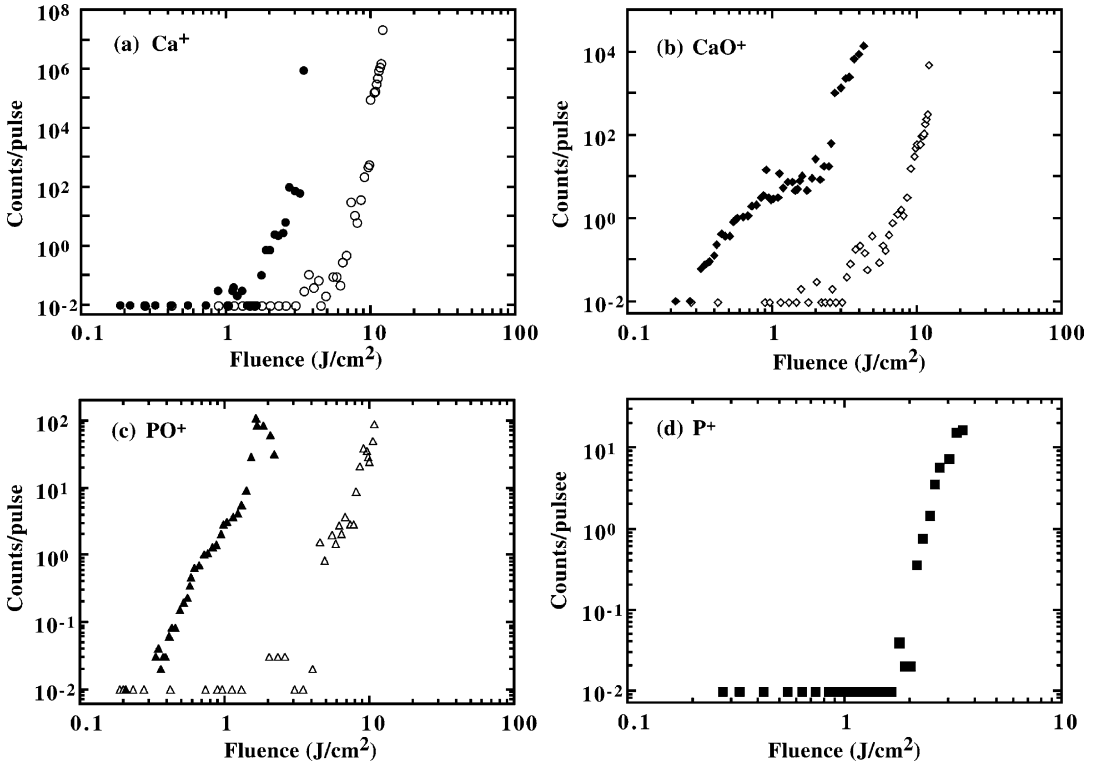

Fig. 1. Fluence dependence of the intensities of the principal ion emissions from as-cleaved brushite: (a) Ca^+; (b) CaO^+; (c) PO^+; and (d) P^+, before (open symbols) and after (filled symbols) electron irradiation.

electron-irradiated surface, as shown in Fig. 2. Similar structures are observed on the surfaces of brushite crystals heated to 100 °C in air in an oven [36]. Images taken at higher magnifications (Fig. 2(b) and (c)) show that many of these exposed voids are lined with small plate-like crystals.

These rough, defect-laden surfaces are expected to absorb strongly at the laser wavelength and yield intense emission. The formation of $P_2O_7^{4-}$ on the HPO_4^{2-} sublattice should result in high densities of anion defects, such as HPO^{4-} vacancies. These vacancies are similar to F-centers in the alkaline earth oxides. $P_2O_7^{4-}$ vacancies on damaged brushite surfaces are potentially more efficient electron traps than HPO_4^{2-} vacancies, being able to trap up to twice as many electrons. $P_2O_7^{4-}$ vacancies and related complex anion defects would serve as sorption and emission sites, significantly reducing the observed "threshold fluences" for ion emission from electron-irradiated surfaces.

In addition to thermally-induced changes, electron irradiation produces additional chemical effects. The production of P^+ and P° from electron-irradiated surfaces, and their absence from as-grown and as-cleaved surfaces, is strong evidence for chemical reduction of surface species. The high electron and excitation densities near the surface during electron irradiation would naturally provide a strongly reducing chemical environment. A reducing environment may also enhance $P_2O_7^{4-}$ production, with the attendant emission of O_2 ($P_2O_7^{4-}$ can also be produced by simple heating).

3.3. UV laser-induced neutral emission

One might expect water to be a major neutral product from hydrated crystals. Following any reasonable pumpdown, however, the H_2O signals accompanying laser irradiation at 248 nm laser are barely detectable. The dehydration of the near-surface region

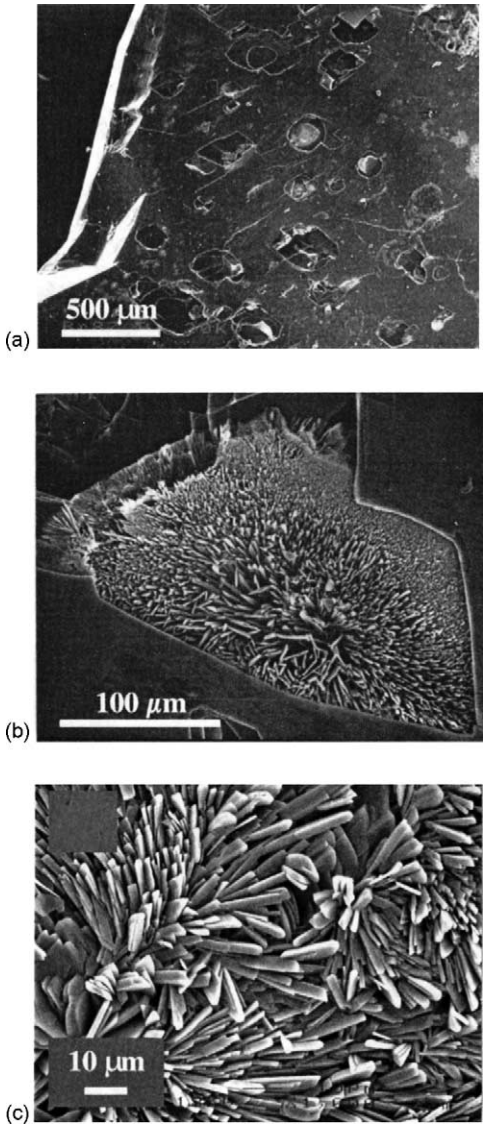

Fig. 2. SEM micrographs of an electron-irradiated surface: (a) entire irradiated region; (b) close up of exposed interior material; (c) view of recrystallized material at a still higher magnification. These rough regions are "hot-spots" for both ion and neutral emissions due to high defect densities.

of the crystal is clearly evident in the background mass spectrum. Thus the surface is presumably transformed to $CaHPO_4$; this transformation is supported by XPS measurements on evacuated brushite samples [35]. Laser-induced neutral emissions on the resulting surfaces are difficult to observe in the absence of electron- or laser-induced damage. These samples do show weak neutral O_2 and some neutral Ca. The latter signal typically depletes with repeated laser pulses at modest fluences, indicating that the associated defect sites are destroyed faster than they are created by the laser.

After electron irradiation at doses of 0.1–2.8 C/cm^2, laser irradiation produces neutral Ca, CaO, O_2, PO_2, PO, and P emissions. Typical TOF curves for these emissions, before and after electron irradiation, are shown in Fig. 3. Electron doses and laser fluences were not exactly the same for each species; at this stage we are most interested in determining if the electron beam influenced the emission intensities which it clearly does.

Electron irradiation increases O_2 and Ca signals more than an order of magnitude (at the same laser fluence). For a given laser fluence, the electron dose required to achieve reasonable neutral Ca signals is nearly an order of magnitude higher than for the other species. The TOF curves (really, "time-of-arrival") for Ca, CaO, PO, and PO_2 are well fit by Maxwell–Boltzmann distributions. Atomic P emission curves are generally too small for reliable curve fitting. Curve fits for the four significant neutral emissions are shown in Fig. 4, along with the resulting "best fit" temperatures. We wish to emphasize that on all ionic crystals studied to date in our laboratory, the neutral products all exhibit thermal behavior at wavelengths corresponding to photon energies below the band gap. Defects are the only reasonable absorbers to initiate such a process.

Obviously, the temperature rise and fall accompanying the laser pulse is not constant in time. If, however, the emission mechanism is thermal, the highest temperatures dominate, so that the range of temperatures (and time) of significant emission is rather narrow. Consequently, the time-of-flight curves will correspond to a δ-function in time and a single temperature. The good agreement among the four temperatures shown here is consistent with thermal desorption from surfaces with well defined temperatures.

3.4. More extensive electron beam exposure

By extending the time of exposure to the electron beam to several minutes we found that the brushite surface became even rougher. Close examination of

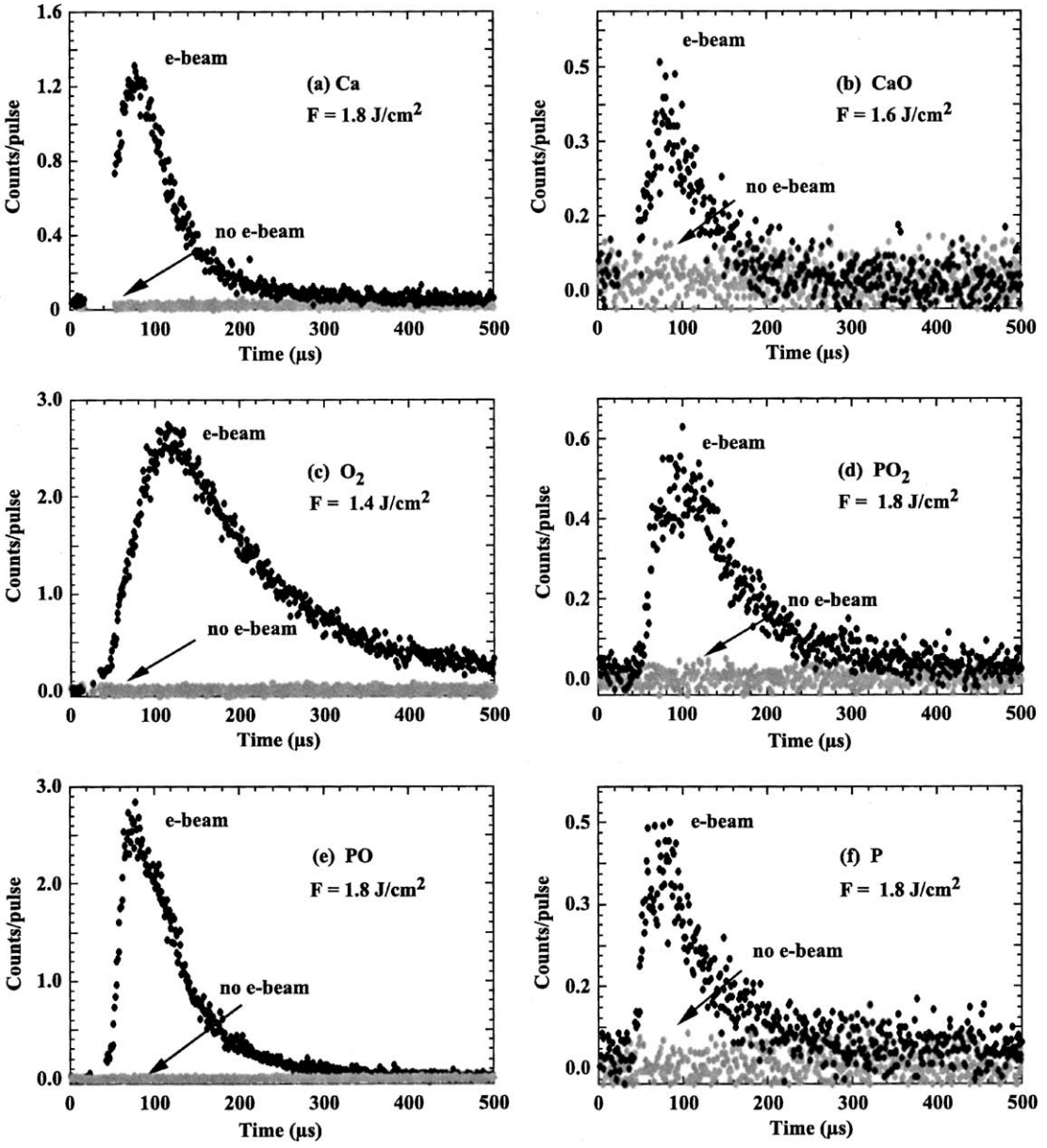

Fig. 3. Neutral emission time-of-flight curves before and after a 0.8 C/cm^2 dose of 2 keV electrons: (a) Ca; (b) CaO; (c) O_2; (d) PO_2; (e) PO; and (f) P. The laser fluence for each species was chosen to produce significant emission. Basically, at these fluences, no neutral emission is observed without electron bombardment.

this surface showed us that in parts of the surface where structures were in poor thermal contact with the main crystal body (overhangs of the craters and the platelets grown in the cavities), high aspect ratio cones were generated. Typical images of these structures are shown in Fig. 5. The cones are often 2–5 μm in length and end with tips with radii on the order of 100 nm or less. An important aspect of the mechanism for this cone formation is revealed at places where one platelet on the surface partially shields another from the

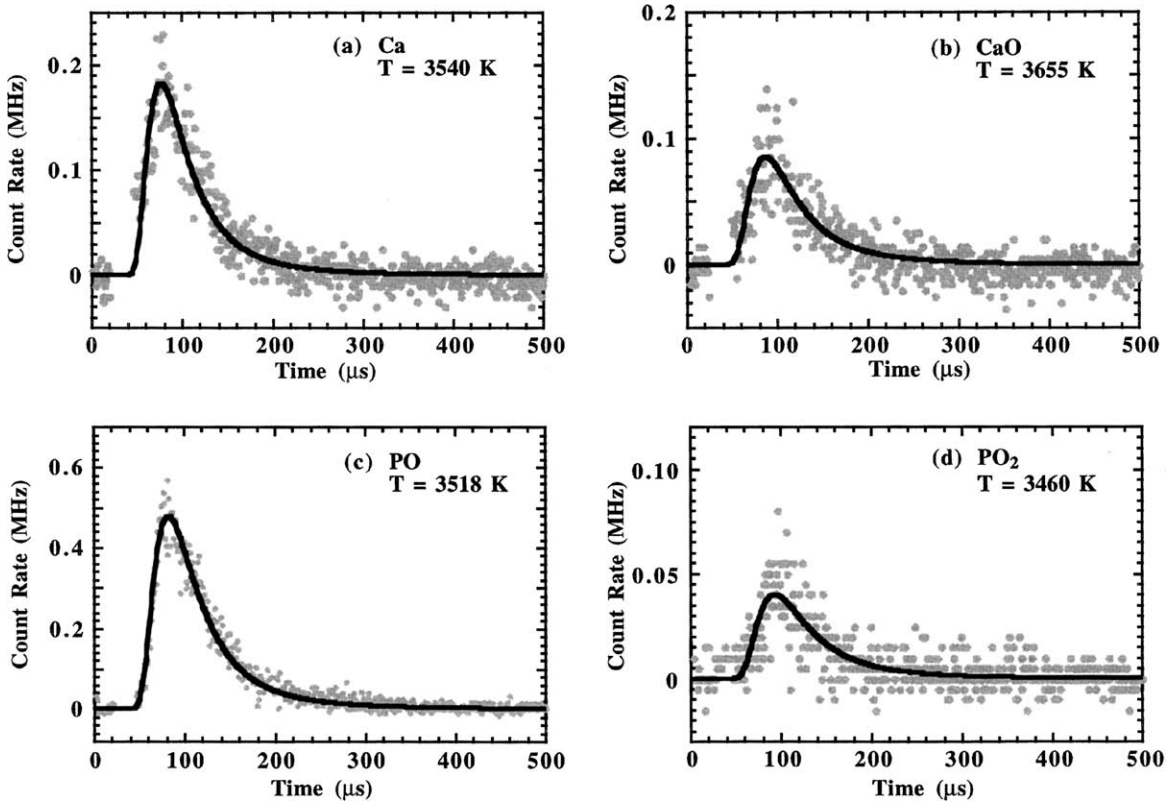

Fig. 4. Neutral product time-of-flight signals from the same site and laser fluence for: (a) Ca; (b) CaO; (c) PO; and (d) PO_2. Note that all of the best fit Maxwell–Boltzmann distributions correspond to similar temperatures.

electron beam. Such a region is seen in Fig. 6. In the shadow, the original surface can be seen unaffected by the beam. As one goes out from the shadow, the current density increases continuously. The entire exposed region is recessed relative to the unexposed region and the cones are seen to be highest in the weaker beam and lower in the region receiving the full current density. This proves conclusively that cone formation involves an etching process as opposed to a growth process.

The heating of these structures that are poorly attached to the bulk of the crystal is also an important part of the mechanism. We hypothesized that the major etching mechanism is a thermally assisted electronic process, namely electron stimulated desorption/decomposition (ESD) [37–39]. With our mass spectrometer (MS), we were able to measure the neutral gaseous products generated during irradiation and found in decreasing order of intensity: O_2, P, PO, PO_2, Ca, and PO_3. Assuming cosine angular distributions for all of the emissions, the MS data could be quantified and integrated to provide a total loss of material during the beam exposure. Estimates of the material volume lost were made from the SEM photographs, such as those above. Comparing these two measurements confirmed that the gasification of the sample accounted for the missing material.

To confirm that heating was indeed important, we mounted small flakes of brushite on a sample holder that could be heated to 70 °C. Fig. 6(b) shows the resulting cone formation on such a flake (∼15 μm in diameter). The dose used to generate these cones was far smaller, ∼1/100th that of what was needed on the bulk brushite surface. This is due to a dramatic increase in the rates of ESD at elevated temperatures. For simpler substrates such as alkali halides this

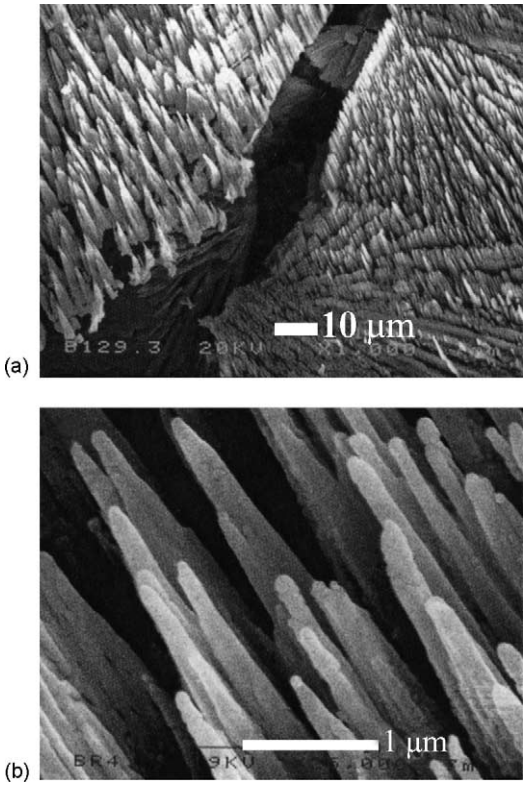

Fig. 5. Cones formed by extensive irradiation of brushite cleavage surfaces by 2 keV electrons (dose = 2.5 C/cm^2). The arrays of cones tend to occur in rows along surface crystallographic directions and the cones point in the direction of the incident electron beam. They often have lengths of several microns and end in radii ~100 nm or less.

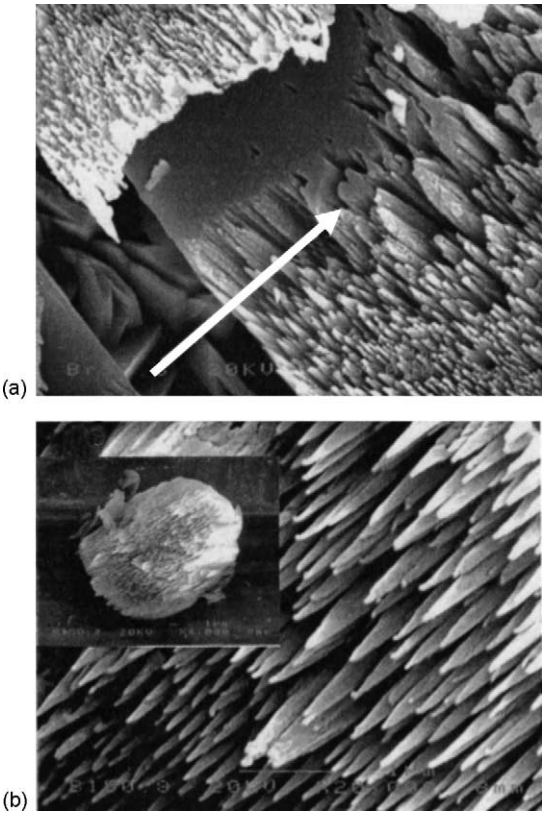

Fig. 6. (a) Cones generated on two overhanging platelets on bulk brushite. The bottom sheet is shielded from the electron beam by the overhang above showing that cone formation is an erosion process rather than a growth process. (b) Cone formation on a small flake of brushite (insert shows an irradiated flake 15 μm in diameter) attached to a heater. Irradiation was carried out at 55 °C; the dose (and therefore the time) required to produce cones was ~1/100 of that required on the bulk brushite surface.

thermal aspect is understood (see later). For brushite we are not yet sure what the thermally activated step is that determines this behavior. Nevertheless, this simple experiment shows that steady state heating leads to enhanced rates of cone formation. Note that again the direction of the cone orientation is towards the incident electron beam.

The XPS and FT-IR studies mentioned earlier suggest that the outer regions of these structures are reduced, tending towards dehydrated pyrophosphate. This material is more robust and is likely to be more resistant to decomposition. Furthermore, this happens first on the outer most surfaces where more electron density is received.

From the above observations we propose the following scenario for cone formation:

(a) Initially, ESD on a nearly perfect substrate begins to form point defects; aggregation of such defects initiates a roughening of the surface.
(b) Through anion decomposition, the material towards the top is more resistant to decomposition and can form capstones that will cause strong heterogeneity in etch rates favoring cone formation.
(c) Preferential etching occurs in the depressed regions; charging of the top parts of the emerging cones could also help channel electrons down into the regions around the cones. Obviously, the direction of the incoming electrons sets the preferred regions that get etched the fastest, thus the directionality of the cones.

3.5. Adding water vapor to "dry crystals"

We now consider the influence of background water in the vapor phase during irradiation of two inorganic crystals not containing hydrated water, NaCl and $NaNO_3$. During e-beam irradiation at 10^{-7} Pa versus 10^{-5} Pa partial pressure H_2O, significant increases in the ESD yields for these two materials was observed in the presence of water vapor. We show this effect for NaCl in Fig. 7, where we also varied the temperature of the crystals. Both stimuli, particularly in combination, cause increases in the neutral species (Na, Cl, and two isotopic masses of Cl_2).

From the temperature dependence we can use Arrhenius plots to determine an activation energy (E_a), for each of the products. The fits are surprisingly consistent and yield the *same value for all of the products*, namely 0.075 ± 0.01 eV. Similar measurements of intensity, "wet" and "dry" and versus temperature have been carried out for the e-beam products from $NaNO_3$ and for 248 nm laser irradiation of both NaCl and $NaNO_3$. For illustration, in Fig. 8 we show the Arrhenius plots for the laser-induced neutral emissions at 60 mJ/cm^2 fluence from NaCl—for all products and both wet and dry we obtain the same activation energy as with electrons: 0.075 eV. The $NaNO_3$ activation energies are also constant for all detected products and average slightly higher than for NaCl, namely 0.09 ± 0.01 eV. We have been able to identify from the literature a process that corresponds to the measured E_a for NaCl, namely a thermally activated step in F-center formation. F-center formation

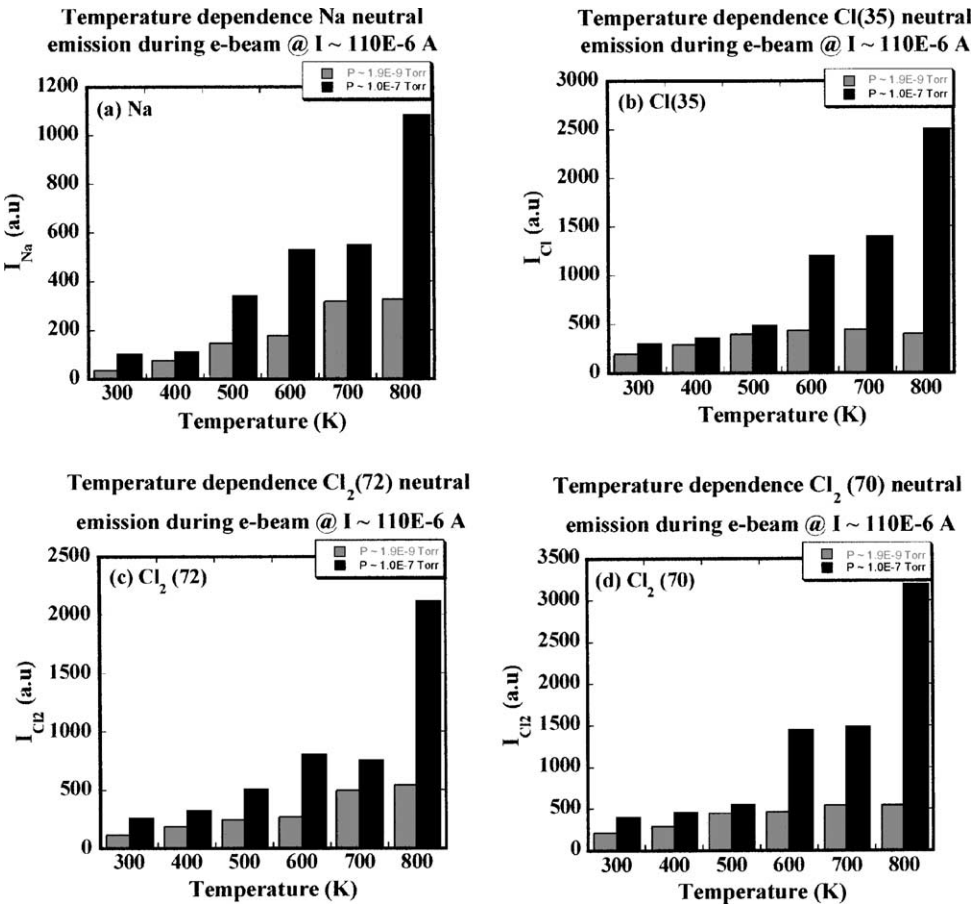

Fig. 7. The emission intensities of the neutral species seen from cleaved NaCl in $\sim 10^{-7}$ Pa background and in 10^{-5} Pa water vapor for temperatures ranging from 300 to 800 K. The presence of water can enhance the yields by as much as a factor of 6.

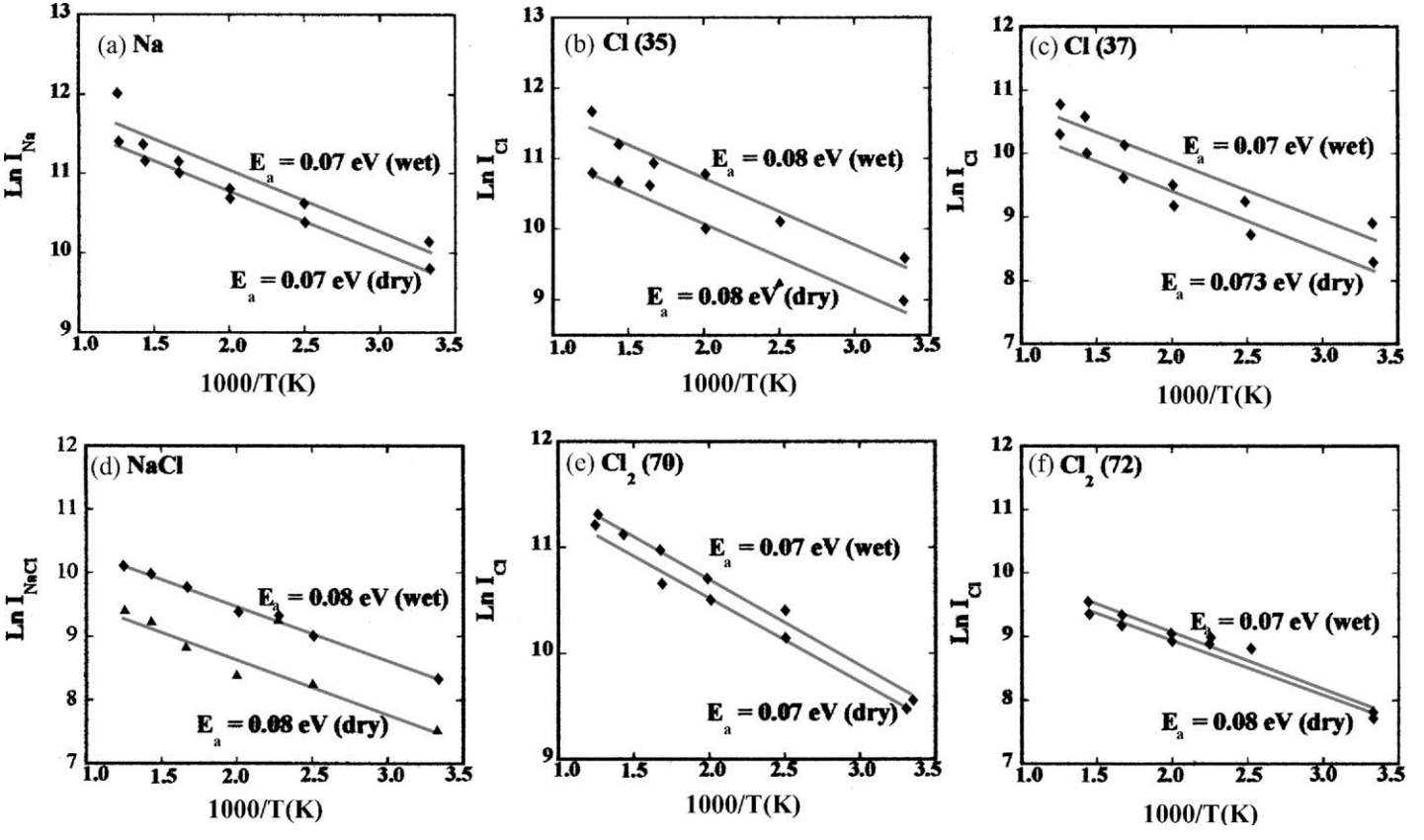

Fig. 8. Arrhenius Plots for the neutral species from 248 nm laser irradiated NaCl(1 0 0) at a laser fluence of 60 mJ/cm^2.

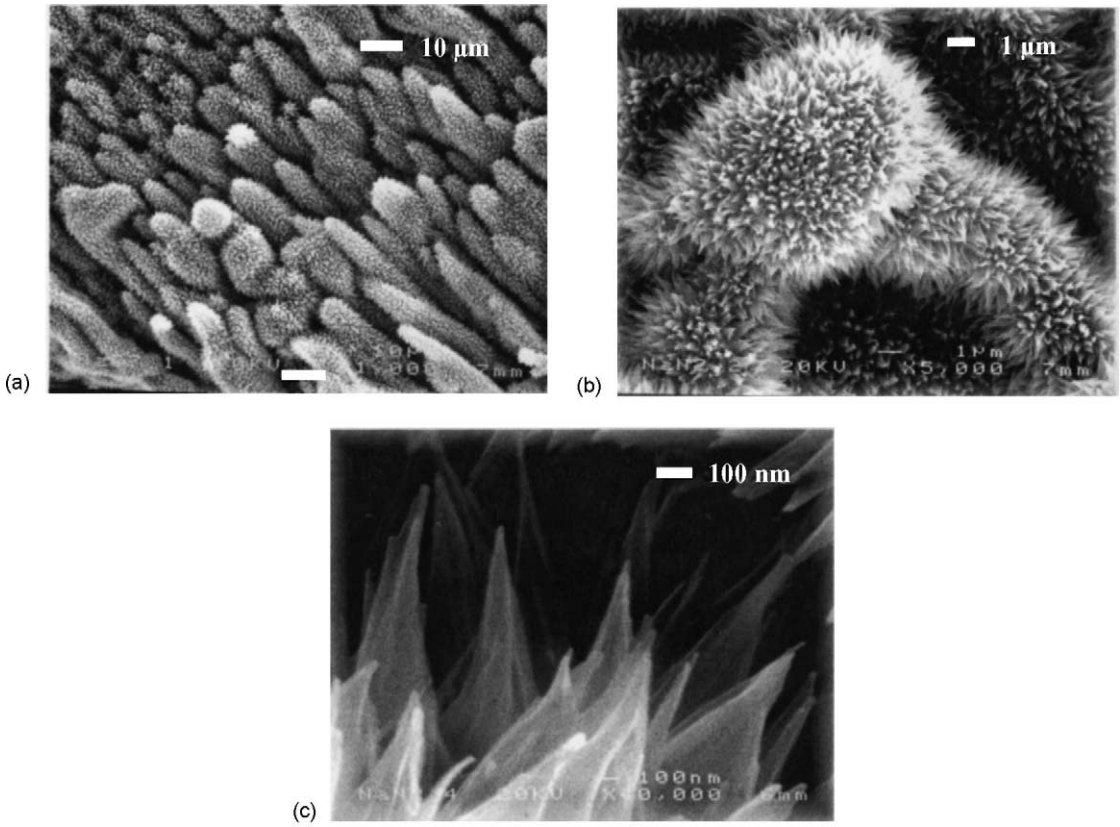

Fig. 9. SEM images of e-beam irradiated $NaNO_3$ surfaces showing the diverse structures generated by 2 keV electrons (dose ~0.9 C/cm^2) in 2×10^{-5} Pa partial pressure of water vapor.

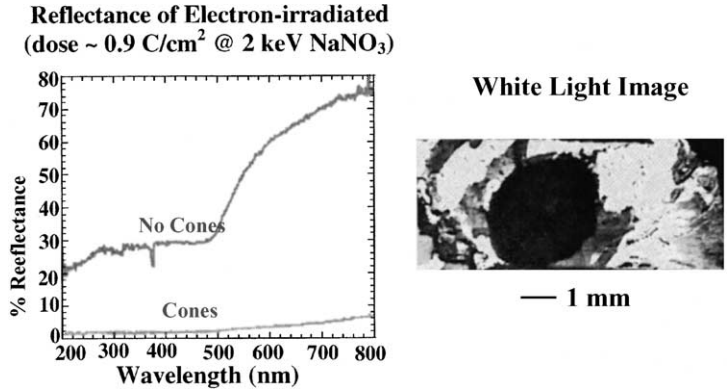

Fig. 10. Reflectivity vs. wavelength of the surface (gold coated) corresponding to the surfaces shown in Fig. 9. A white light image of the surface is shown also—the black spot is the e-beam irradiated region.

in the alkali halides in general and NaCl in particular has been especially well studied (see [40]). A self-trapped exciton at a Cl^- site can decay to form an F-center/H-center pair (anion vacancy adjacent to a Cl_2^- center) when the Cl° at the exciton site hops to a nearest neighbor Cl^- site. This hop is thermally activated, with an activation energy of 0.07 eV—consistent with the 0.075 ± 0.01 eV activation energies observed here.

Finally, we show an example in Fig. 9 of the rich topography generated on $NaNO_3$ by extensive e-beam irradiation in a background of 10^{-5} Pa water vapor. This surface is highly light absorbing due to its extremely high tortuosity (light cannot make it back out!). We call it our ''stealth surface''. Even when gold coated, the measured reflectivity in the electron-irradiated region is near zero from 500 nm down to below 200 nm (see Fig. 10).

4. Conclusion

We have shown how systems containing water of hydration ($CaHPO_4{\cdot}2H_2O$) or those with an affinity for water ($NaNO_3$, NaCl) result in unique interactions with electron and laser radiation. For brushite, the waters of hydration strongly influence the formation of voids via thermally-induced segregation of water resulting in fracture of the lattice. These voids form incubators for effluorescence-driven recrystallization. Further e-beam irradiation leads to nanometer scale cone formation through extensive ESD driven erosion. ''Dry'' (non-hydrated) crystals with some affinity for water show dramatic increases in sensitivity to both e-beam and laser irradiation at relatively low (10^{-5} Pa) partial pressures of water vapor. Simultaneously heating the crystal enhances this process for both types of radiation and exhibits the same activation energies (E_a) for all the products detected. In the case of NaCl, the value of 0.075 eV corresponds closely to the energy required for thermally assisted F-center formation. Structures observed on these non-hydrated crystals are noteworthy and span a size range from several microns down to a few nm. Accordingly, they form strong optical absorbers in the visible and near UV. In general we anticipate interesting consequences from continued studies of combined exposure of surfaces to radiation and slightly aggressive chemicals.

Acknowledgements

We thank Loren Cramer, WSU, for help in the laboratory and Richard Haglund, Vanderbilt University for helpful discussions. This work is supported by the US. Department of Energy under Grant no. DE-FG03-98ER14864 and by the National Science Foundation KDI Grant DMR-9980015.

References

[1] J.T. Dickinson, L.C. Jensen, M.L. Klakken, J. Vac. Sci. Technol. A 4 (1986) 1501.
[2] J.T. Dickinson, K. Tonyali, M.L. Klakken, L.C. Jensen, J. Vac. Sci. Technol. A 5 (1987) 1076.
[3] J.T. Dickinson, M.A. Loudiana, A. Schmid, in: L.H. Lee (Ed.), Adhesion, Sealants and Coatings for Space and Health Environments, Plenum Press, New York, 1987, p. 467.
[4] M. Guardalben, A. Schmid, M. Loudiana, J.T. Dickinson, Phys. Rev. B 35 (1987) 4026.
[5] S.C. Langford, J.T. Dickinson, L.C. Jensen, J. Appl. Phys. 62 (1987) 1437.
[6] M.A. Loudiana, J.T. Dickinson, A. Schmid, E.J. Ashley, Appl. Surf. Sci. 28 (1987) 311.
[7] J.T. Dickinson, Surface Interactions Relevant to Space Station Contamination Problems, 3002 National Aeronautics and Space Agency, 1988.
[8] J.T. Dickinson, S.C. Langford, L.C. Jensen, P.A. Eschbach, L.R. Pederson, D.R. Baer, J. Appl. Phys. 68 (1990) 1831.
[9] J.T. Dickinson, J.-J. Shin, S.C. Langford, Appl. Surf. Sci. 96–98 (1996) 326.
[10] M. Dawes, S.C. Langford, J.T. Dickinson, Appl. Surf. Sci. 127–129 (1998) 81.
[11] S. Nakahara, S.C. Langford, J.T. Dickinson, Tribol. Lett. 1 (1995) 277.
[12] N.-S. Park, M.-W. Kim, S.C. Langford, J.T. Dickinson, Langmuir 12 (1996) 4599.
[13] R.F. Hariadi, S.C. Langford, J.T. Dickinson, J. Appl. Phys. 86 (1999) 4885.
[14] L. Scudiero, S.C. Langford, J.T. Dickinson, Tribol. Lett. 6 (1999) 41.
[15] M.J. Stirniman, C. Huang, R.S. Smith, S.A. Joyce, B.D. Kay, J. Chem. Phys. 105 (1996) 1295.
[16] R. Schaub, P. Thostrup, N. Lopez, E. Lægsgaard, I. Stensgaard, J.K. Nørskov, F. Besenbacher, Phys. Rev. Lett. 87 (2001) 266104.
[17] R.Z. LeGeros, J.P. LeGeros, J. Crystal Growth 13–14 (1972) 476.
[18] C. Bandis, L. Scudiero, S.C. Langford, J.T. Dickinson, Surf. Sci. 442 (1999) 413.
[19] S. Aduru, S. Contarini, J.W. Rabalais, J. Phys. Chem. 90 (1986) 1683.
[20] H. Yamashita, R. Kato, J. Phys. Soc. Jpn. 29 (1970) 1557.
[21] H. Yamashita, J. Phys. Soc. Jpn. 33 (1972) 1407.

[22] M. Kamada, R. Kato, J. Phys. Soc. Japan 35 (1973) 1561.
[23] V.N. Voitsekhovskii, V.P. Nikolaeva, L.I. Venevtseva, E.A. Sidorova, Sov. Phys. Crystallogr. 30 (1985) 360.
[24] J.T. Dickinson, in: J.C. Miller, R.F. Haglund (Eds.), Experimental Methods in Physical Sciences, vol. 30, Academic Press, New York, 1998, p. 139.
[25] J.T. Dickinson, S.C. Langford, J.J. Shin, D.L. Doering, Phys. Rev. Lett. 73 (1994) 2630.
[26] D.R. Ermer, J.-J. Shin, S.C. Langford, K.W. Hipps, J.T. Dickinson, J. Appl. Phys. 80 (1996) 6452.
[27] S. Kano, S.C. Langford, J.T. Dickinson, J. Appl. Phys. 89 (2001) 2950.
[28] C.A. Beevers, Acta Cryst. 11 (1958) 273.
[29] L. Backbier, J. Rousseau, Anal. Chim. Acta 283 (1993) 855.
[30] L.T. Gibson, B.G. Cooksey, D. Littlejohn, N.H. Tennent, Anal. Chim. Acta 337 (1997) 151.
[31] E. Ordonez, J. Twilley, Anal. Chem. 69 (1997) 416A.
[32] A.G. Verduch, V. Sanz, J.V. Agramunt, V. Beltrán, Am. Ceram. Soc. Bull. 75 (1996) 60.
[33] T. Vickers, M. Moukwa, J. Testing Eval. 24 (1996) 80.
[34] P. Zanetta, M. Facchini, Optics Commun. 104 (1993) 35.
[35] J.T. Dickinson, S.C. Langford, C. Bandis, M.L. Dawes, Y. Kawaguchi, Appl. Surf. Sci. 154–155 (2000) 291.
[36] Y. Kawaguchi, M.L. Dawes, S.C. Langford, J.T. Dickinson, Appl. Phys. A 69 (1999) S621.
[37] M.L. Knotek, P.J. Feibelman, Phys. Rev. Lett. 40 (1978) 964.
[38] R. Gomer, in: N.H. Tolk, M.M. Traum, J.C. Tully, T.E. Madey (Eds.), Desorption Induced by Electronic Transitions DIET I, Springer, Berlin, 1983, p. 40.
[39] R.D. Ramsier, J.T. Yates, Surf. Sci. Rep. 12 (1991) 246.
[40] N. Itoh, M. Stoneham, Materials Modification by Electronic Excitation, Cambridge University, Cambridge, UK, 2000 (and references therein).